Hybrid plasma-thermal system for methane conversion to ethylene and hydrogen

Hybrid Plasma-Thermal System for Methane Conversion to Ethylene and Hydrogen

Rui Liu [1], Yingzi Hao [1], Tong Wang [1], Li Wang [2], Annemie Bogaerts [3], Hongchen Guo [1]*, and Yanhui Yi [1]*

[1] State Key Laboratory of Fine Chemicals, School of Chemical Engineering, Dalian University of Technology, Dalian 116024, Liaoning, China

[2] College of Environmental Sciences and Engineering, Dalian Maritime University, Dalian 116026, Liaoning, China.

[3] Research group PLASMANT, Department of Chemistry, University of Antwerp, Universiteitsplein 1 BE-2610 Wilrijk-Antwerp, Belgium.

Corresponding Author

*Yanhui Yi. E-mail: yiyanhui@dlut.edu.cn

*Hongchen Guo. E-mail: hongchenguo@163.com

Abtract: By combining dielectric barrier discharge plasma and external heating, we exploit a two-stage hybrid plasma-thermal system (HPTS), i.e., a plasma stage followed by a thermal stage, for direct non-oxidative coupling of CH_4 to C_2H_4 and H_2, yielding a CH_4 conversion of ca. 17 %. In the two-stage HPTS, the plasma first converts CH_4 into C_2H_6 and C_3H_8, which in the thermal stage leads to a high C_2H_4 selectivity of ca. 63 % by pyrolysis, with H_2 selectivity of ca. 64 %.

Key Words: hybrid Plasma-Thermal System; methane conversion; ethylene; hydrogen

Introduction

Methane conversion, a thermodynamically unfavorable process, requires high temperature and catalysts. Usually, the direct conversion into C_2 hydrocarbons has been investigated by oxidative coupling of methane (OCM) and nonoxidative coupling of methane (NOCM). Although OCM is a much better option in terms of C_2 hydrocarbons yield, [1-4] a large amount of CO_x and a low efficiency of methane utilization have been obtained. For the NOCM, the overoxidation of methane and C_2 hydrocarbons can be prevented, and H_2 can be produced as a desired product instead of H_2O in OCM. Therefore, NOCM to ethylene (C_2H_4) is a promising route for CH_4 conversion, which has been achieved by thermal pyrolysis,[5] catalytic methods[5-8] and plasma-based approaches.[9,10]

Due to the high stability of the C-H bond in CH_4, thermal pyrolysis is typically operated at extremely high temperature, which leads to high selectivity of solid carbon (>90%), but low selectivity toward C_2 hydrocarbons (<10 %).[5,11] Recently, Bao et al. presented a Fe©SiO_2 catalyst with single atomic iron sites confined in silica matrix, being promising for CH_4 conversion to produce ethylene and aromatics. 48 % CH_4 conversion was maintained in a 60 hour stability test at 1100 ^oC.[5] Varma et al. described that ZSM-5 zeolite supported bimetallic Pt-Bi catalysts stably and selectively convert methane (< 1 %) to C_2 species with high selectivity (> 90 %) at relatively moderate temperatures (600−700 °C).[11] Dumesic et al, reported Pt and PtSn catalysts supported on SiO_2 and H-ZSM-5 for methane conversion under nonoxidative conditions at 1123 K.[12] Although the reaction temperature has been reduced by the catalytic approach, the methane non-oxidative coupling still needs to be operated at temperatures higher than 1000 ^oC to obtain reasonable CH_4 conversion (Table S1). Plasma has been combined with catalysts for methane non-oxidative coupling at lower temperature to obtain high CH_4 conversion, even at ambient

temperature.[13-15] In plasma, the energetic electrons can effectively activate CH_4 molecule to produce abundant chemically active species such as radicals and excited species through electron-molecule collisions ($CH_4 + e \rightarrow CH_3 + H + e$; $CH_4 + e \rightarrow CH_2 + H_2 + e$). The generated active species can rapidly react with each other to produce hydrocarbons at atmospheric pressure. However, either C_2H_6 or C_2H_2 was obtained as the main product, and C_2H_4 can be obtained with satisfied selectivity only in the case of placing Pd-based hydrogenation catalysts in the post-plasma region of thermal plasma (C_2H_2 hydrogenation to C_2H_4).[16-18] Thermodynamic calculation of CH_4 pyrolysis (Figure S1) indicates that C_2H_4 can be produced as the dominant product at a temperature around 800 °C with CH_4 conversion lower than 10 %. Therefore, the combination of plasma chemistry and thermal pyrolysis may be a promising approach for CH_4 to C_2H_4 conversion with high selectivity and CH_4 conversion, but it has never been explored.

Herein, by combining dielectric barrier discharge (DBD) plasma and external heating, we exploited a hybrid plasma-thermal system (HPTS) for direct non-oxidative coupling of CH_4 to C_2H_4 (Figure S2). Our results demonstrate that one-stage HPTS shows C_2H_4 selectivity of 80 %, but CH_4 conversion of only 2 %. However, two-stages HPTS (plasma stage followed by thermal stage) exhibits not only high C_2H_4 selectivity of ca. 63 % but also a CH_4 conversion of ca. 17 %, suggesting an excellent potential for practical conversion of CH_4 to C_2H_4 and H_2.

Results and Discussion

Figure 1a shows the schematic diagram of the one-stage HPTS. The DBD reactor was heated by a furnace, aiming to control the bulk reaction temperature, which was monitored by thermocouple for NOCM to C_2H_4 from 200 °C to 880 °C. Furthremore, the temperature was also recorded by a thermal infrared imager (Figures S3-S5), which demonstrate that the temperature measured by

thermocouple was nearly consistent with that of thermal infrared imager within the detection limit. Figure 1b illustrates that, in this one-stage HPTS, higher temperatures (heated by the furnace) lead to lower specific energy input (SEI), since the electric field of the DBD was weakened by the high temperature, resulting in extremely weak discharges. This can be demonstrated by the measured discharge currents (Figure S6b) and discharge voltages (Figure S6a), and the discharge power calculated by Lissajous figures (Figure S6c). The most plausible reason for the weak discharge at high temperature (> 400 °C) is that the resistance of methane gas decreases with increasing temperature, and most of energy is therefore consumed by power supply with a relative high resistance.[19] The results in Figure 1b reveal that the SEI is inversely proportional to the reaction temperature in this one-stage HPTS, and elevated temperatures lead to low SEI.

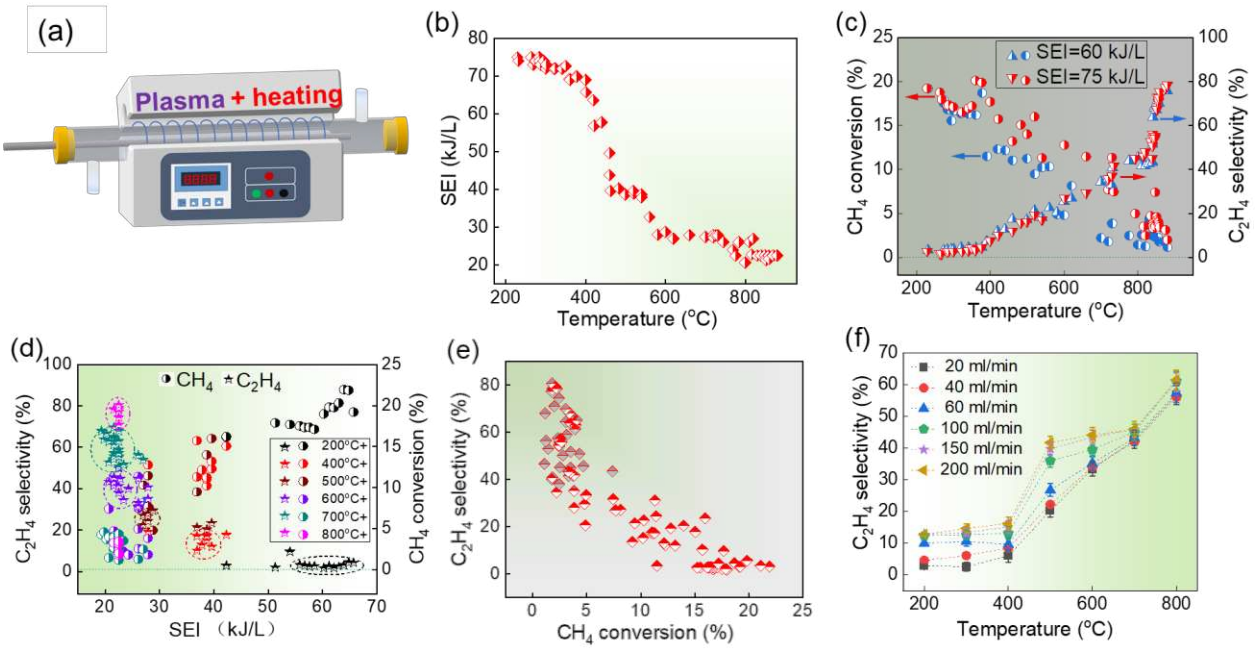

Figure 1. Performance of the one-stage hybrid plasma-thermal system (HPTS) for methane to ethylene conversion. (a) schematic diagram of one-stage HPTS; (b) relationship of temperature and SEI; (c) CH_4 conversion and C_2H_4 selectivity as a function of temperature; (d) CH_4 conversion and C_2H_4 selectivity as a function of SEI; (e) CH_4 conversion versus C_2H_4 selectivity; (f) effect of total flow rate on C_2H_4 selectivity.

Figure 1c depicts the CH_4 conversion and C_2H_4 selectivity as a function of reaction temperature with a initial SEI without external heating (60 or 75 kJ/L). The CH_4 conversion gradually drops, while the C_2H_4 selectivity gradually rises. Specifically, significant CH_4 conversion (10-20 %) is achieved below 400 °C with extremely low C_2H_4 selectivity (< 10 %), similar to the performance of "DBD only" (without external heating), with C_2H_6 as the main product (Figure S7). In case of high temperature (especially higher than 800 °C), the one-stage HPTS shows high C_2H_4 selectivity (50-80 %) but low CH_4 conversion (ca. 2 %). The corresponding results of H_2 selectivity are shown in Figure S8. The CH_4 conversion is now similar to the performance of thermal pyrolysis (Figure S9), which means that the weak discharge at high temperature in the one-stage HPTS does not help for dissociation of the C-H bond and activation of CH_4. However, the C_2H_4 selectivity is around 40 times higher than the performance of thermal pyrolysis at the same temperature (where coke is the dominant product, as shown in Figure S9). This result suggests a complex interaction between DBD plasma and external heating in the one-stage HPTS, i.e., regulating radical species and reaction pathways, which are likely responsible for the enhancement of C_2H_4 selectivity at high temperature.

Figure 1d illustrates the reaction performance at different SEI with fixed reaction temperature. Generally, upon increasing SEI, the CH_4 conversion rises but the C_2H_4 selectivity drops, and the highest C_2H_4 selectivity (ca. 82 %) is achieved at 880 °C with 35 kJ/L SEI (Figure S10). Figure 1e shows the correlation between CH_4 conversion and C_2H_4 selectivity, which demonstrates a trade-off relationship. That is, we cannot achieve high CH_4 conversion and high C_2H_4 selectivity simultaneously in one-stage HPTS. This trade-off also applies to one-stage HPTS at different flow rates, i.e., Figure 1f and Figure S11, in which the experimental uncertainty are shown as error bar. The intrinsic reason for this trade-off is that high SEI and high temperature cannot be realized

simultaneously in this one-stage HPTS.

Implementing both high SEI and high temperature is a potential strategy to overcome the trade-off between CH_4 conversion and C_2H_4 selectivity. Thus, we designed a two-stage HPTS, i.e, plasma stage (stage 1) followed by thermal stage (stage 2), as depicted in Figure 2a. Figure 2b shows the performance of the two-stage HPTS with constant SEI in stage 1 (60 kJ/L) but varying temperature in stage 2. Significant and stable CH_4 conversion of ca. 17 % has been achieved at varying temperature. However, the C_2H_4 selectivity increases with rising temperature in stage 2, especially at high temperature (700-880 ^oC). Figure 2c illustrates the performance of the two-stage HPTS with constant temperature (880 ^oC) in stage 2 but varying SEI in stage 1, and the temperature in stage 1 was enhanced by increasing SEI (Figure S12). In this case, significant and stable C_2H_4 selectivity of ca. 60 % has been achieved at varying SEI. However, the CH_4 conversion increased with rising SEI in stage 1. These results indicate that CH_4 conversion was mainly dominated by SEI in stage 1, while C_2H_4 selectivity was mainly managed by temperature in stage 2. The influence of flow rate on methane conversion and ethylene selectivity in the two-stage HPTS is shown in Figure S13, which further demonstrates that high temperature in stage 2 favors C_2H_4 production.

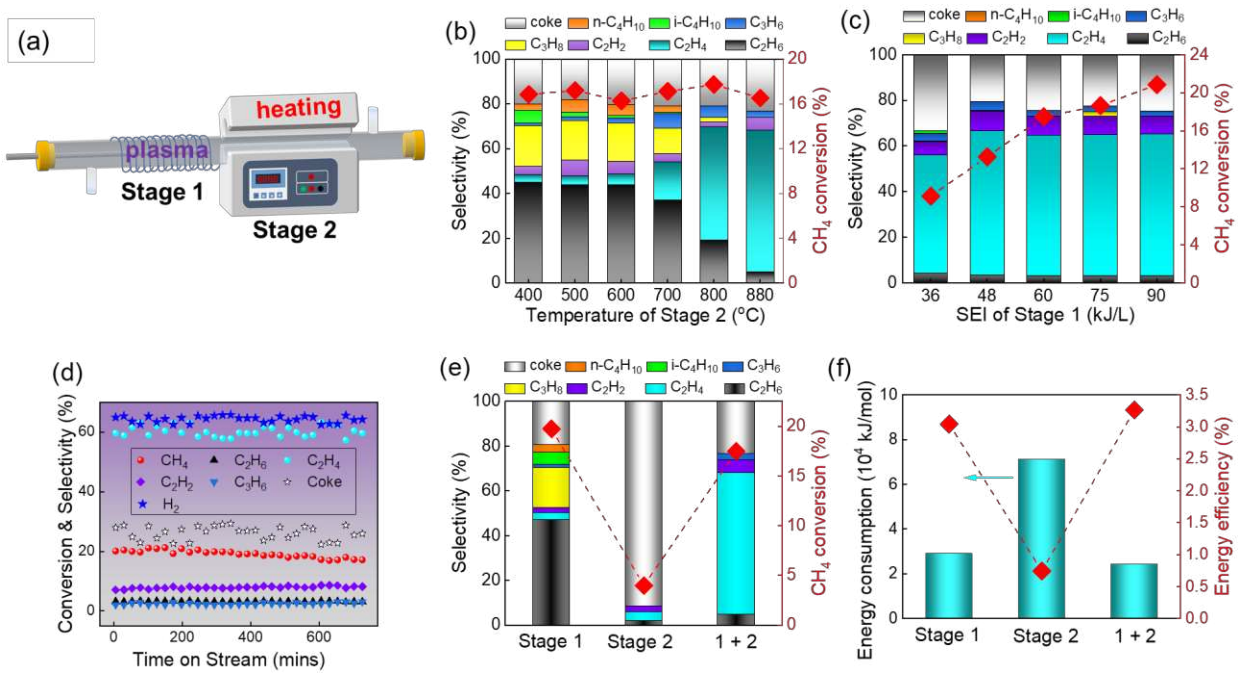

Figure 2. Performance of the two-stage hybrid plasma-thermal system (HPTS) for methane to ethylene conversion. (a) schematic diagram of the two-stage HPTS; (b) effect of temperature in stage 2 on product selectivity and CH_4 conversion at constant SEI (60 kJ/L) in stage 1; (c) effect of SEI in stage 1 on product selectivity and CH_4 conversion at constant temperature (880 °C) in stage 2; (d) reaction stability for the two-stage HPTS for methane to ethylene at constant SEI (60 kJ/L) in stage 1 and constant temperature (880 °C) in stage 2; (e) comparison of CH_4 conversion and product selectivity between "only stage 1", "only stage 2" and "stage 1 + stage 2"; (f) comparison of energy consumption and energy efficiency of main product between "only stage 1", "only stage 2" and "stage 1 + stage 2".

Figure 2d presents the performance of the two-stage HPTS during 12 h continuous operation (at 90 kJ/L, 880 °C). A slightly decline of CH_4 conversion (Figure S14) and stable C_2H_4 selectivity (ca. 60 %) with time on stream suggest an excellent performance and stability of the two-stage HPTS for methane to ethylene conversion. Correspondingly, ca. 64 % H_2 selectivity (based on H balance) has been achieved. Figure 2e summarizes the CH_4 conversion and products distribution in case of "only stage 1" (60 kJ/L), "only stage 2" (880 °C) and "stage 1 + stage 2" (60 kJ/L, 880 °C). The case of "only stage 1" shows C_2H_6, C_3H_8 and i-C_4H_{10} as the main products with ca. 20 % CH_4 conversion. The "only stage 2" case yields coke as the main product with extremely low

conversion of CH_4 (ca. 3.2 %). However, the "stage 1 + stage 2" case shows a satisfying CH_4 conversion (ca. 17 %) and an excellent C_2H_4 selectivity (ca. 63 %). The effect of distance between stage 1 and stage 2 on reaction performance has been investigated, but no obvious effects were found when the distance varied from 1 cm to 20 cm (Figure S15). In addition, compared with "only stage 1" and "only stage 2", the "stage 1 + stage 2" shows a relatively low energy consumption (24.372 MJ/mol$_{C2H4}$) and a relative high energy efficiency (3.263 %), as indicated in Figure 2f. Even so, they are not yet comparable to the state-of-the-art in plasma (1.2 MJ/mol$_{C2H4}$[16]) and catalytic routes (0.8 MJ/mol$_{C2H4}$[5]). This may be caused by the low methane feed flow rate (20 ml/min) and absence of catalysts in the "stage 1 + stage 2" (Figure S15). Therefore, with the increase of methane flow rate, the energy consumption has been reduced and the energy efficiency has been improved a lot (Figure S16 b).

In terms of reactor design, separating the stage1 and stage 2 will increase the cost of setup and operations. However, the economic feasibility of the two-stage HPTS is not only dependant on the above-mentioned costs, but also on the level of scale-up and the performance indexes. Currently, the pilot scale experiment has not been carried out, and thus some commercial data are not available. Therefore, a more detail analysis of economic feasibility will be applied in our further study.

Figure 3 depicts the temporal profiles for various m/z signals obtained by mass spectrometry (MS), corresponding to different species, during "only stage 1", "only stage 2" and "stage 1 + stage 2". In order to accurately record the change of products, the three stages of reactions were operated without interruption. Firstly, CH_4 conversion was operated in a DBD reactor from Plasma-on to Plasma-off, which belongs to Stage 1. After turning off the discharge for ca. 100 min, the heating of the furnace was then initiated until the temperature reached to 880^{o}C, which

belongs to Stage 2. Finally, when the temperature of furnace remained at 880 °C, the discharge in the DBD reactor was turned on (plasma-on). Thus plasma activation and thermal pyrolysis were both turned on, and this belongs to "Stage 1+Stage 2". Clearly, with the transformation from "only stage 1" to "stage 1 + stage 2", the intensity of m/z=28 (which corresponds to C_2H_4 and C_2H_6) became higher, while the intensity of m/z=30 (which only reflects C_2H_6) became much lower. This gives convincing evidence for the switch of the main product from C_2H_6 (only stage 1) to C_2H_4 (stage 1 + stage 2). Furthermore, compared with "only stage 1", the MS profiles also demonstrate more C_2H_2 but less C_3H_8 and C_4 in "stage 1 + stage 2". Correspondingly, in "stage 1 + stage 2", H_2 has been detected by MS with high intensity, which confirms abundant co-production of H_2. These results are consistent with the reaction performance in Figure 2 d and e.

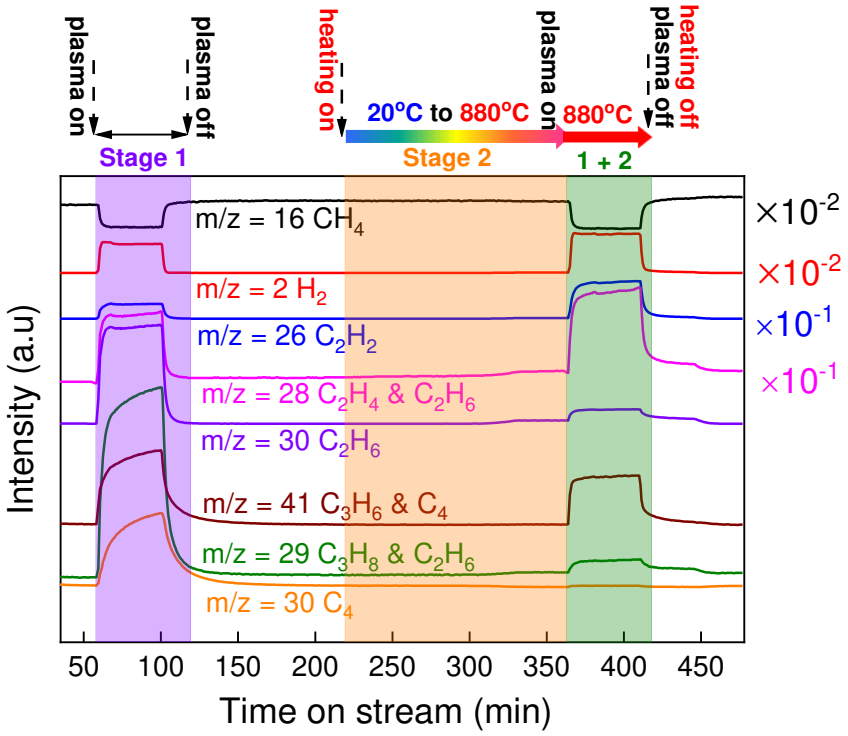

Figure 3. Temporal profiles of MS signals with different m/z values (corresponding to different species), in case of "only stage 1", "only stage 2" and "stage 1 + stage 2".

To reveal how the two-stage HPTS converts CH_4 to C_2H_4 with high selectivity, we studied

the thermal pyrolysis of C_2H_6, C_3H_8 and i-C_4H_{10}, which are the main products from stage 1. Figure S17 shows the reaction performance for thermal pyrolysis of C_2H_6 at different temperatures. Obviously, significant C_2H_6 conversion was achieved only at temperatures higher than 700 ^oC, and the main product is C_2H_4. Figure S18 illustrates similar results, but for thermal pyrolysis of C_3H_8. Again, significant C_3H_8 conversion was achieved only at temperatures higher than 700 ^oC, and the main products consist of C_2H_4, CH_4 and coke. Finally, the results for thermal pyrolysis of i-C_4H_{10} at different temperature, plotted in Figure S19, also demonstrate that significant i-C_4H_{10} conversion was achieved only at temperatures higher than 600 ^oC, and the products consist of coke, C_2H_4, C_3H_6 and CH_4, with coke being the main product.

After analyzing the results in Figure 2 and Figures S16-S19, the temperature corresponding to high C_2H_4 selectivity in Figure 2b is consistent with the temperature for efficient thermal pyrolysis of C_2H_6 and C_3H_8 to C_2H_4 in Figures S17-S18. These results indicate that C_2H_4 in the two-stage HPTS mainly comes from thermal pyrolysis of C_2H_6 and C_3H_8 in stage 2, while C_2H_6 and C_3H_8 originate from plasma-triggered CH_4 coupling in stage 1. However, the coke in the two-stage HPTS mainly arises from thermal pyrolysis of C_3H_8 and C_4H_{10}. Furthermore, a small drop of CH_4 conversion from “only stage 1” to “stage 1 + stage 2” in Figure 2e is mainly caused by thermal pyrolysis of C_3H_8 and C_4H_{10}, which produces again CH_4.

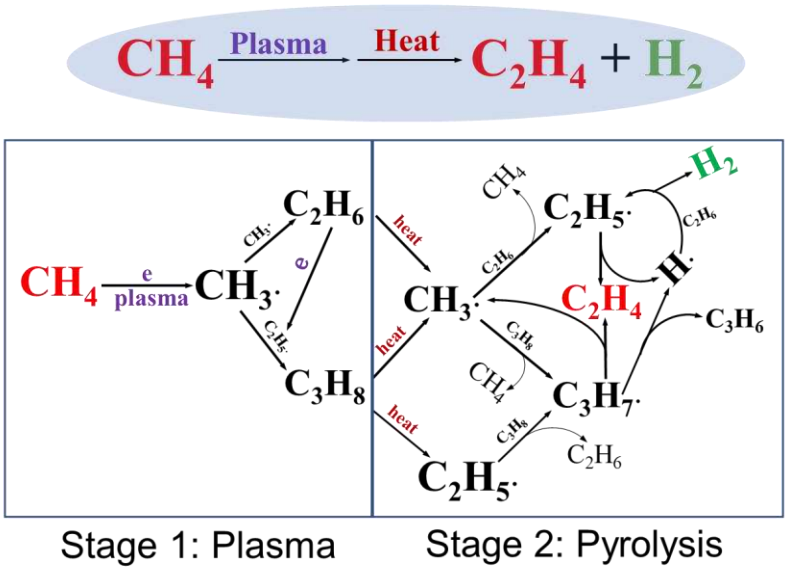

Figure 4. The reaction mechanism of NOCM in the Two-Stage Hybrid Plasma-Thermal System.

A plausible reaction mechanism for CH_4 conversion to C_2H_4 and H_2 in the two-stage HPTS is proposed, as shown in Figure 4. In the plasma (Stage 1), the activation of C-H bond in CH_4 is mainly attributed to the energetic electrons generated by dielectric barrier discharge. Firstly, the energetic electrons transfer their energy to CH_4 molecule through inelastic collisions, leading to the dissociation of C-H bond to form abundant CH_3 radical. Then C_2H_6 can be formed through recombination of CH_3 radicals, leading to the generation of the first main product (C_2H_6) in Stage 1.[20] Meanwhile, the energetic electrons can also dissociate C_2H_6 to generated C_2H_5 radical, which can easily react with CH_3 to produce C_3H_8 as the second main product in Stage 1.[21] Therefore, the main feed gases for stage 2 includes the unreacted CH_4 and the produced C_2H_6 and C_3H_8 from stage 1. Compared with CH_4 thermal cracking at the temperature exceeding 1000 °C, usually, pyrolysis of C_2H_6 and C_3H_8 to form C_2H_4 and C_3H_6 are much easier, and thus they can be operated at a relative lower temperature (Figure S17 and Figure S18). In the pyrolysis of C_2H_6 at high

temperature, the related main reactions are listed in Table S4. Theoretically, both C-C bond and C-H bond can be dissociated to produce CH_3 and C_2H_5 radicals, respectively, which are the chain initiation reactions. However, in C_2H_6 molecule, the bond length of C-C bond and C-H bond are 0.1526 and 0.1101 nm, respectively. This means that C-C bond can be dissociated more easily than C-H bond. That is, the pyrolysis of C_2H_6 is mainly initiated through C-C bond breaking to produce CH_3 radicals, which induce the chain transfer reaction ($CH_3 + C_2H_6 \rightarrow CH_4 + C_2H_5$) to form C_2H_5.[22] Subsequently, C_2H_5 decomposes to produce C_2H_4 and H. After that, H radical leads to a faster chain transfer reaction ($H + C_2H_6 \rightarrow H_2 + C_2H_5$) than CH_3 radical ($CH_3 + C_2H_6 \rightarrow CH_4 + C_2H_5$), since the energy barrier of the former is 9.7 kcal/mol while the later is 16.5 kal/mol. Therefore, $H + C_2H_6 \rightarrow H_2 + C_2H_5$ is the main reaction to consume C_2H_6 for generation of H_2 and C_2H_5, which further produce C_2H_4 through the reaction $C_2H_5 \rightarrow H + C_2H_4$.[22,23] In the thermal cracking of C_3H_8, the related main reactions are listed in Table S5. For C_3H_8 molecule, the length of C-H bond (1.102 nm) is shorter than that of C-C bond (1.528 nm), which means that the breaking of C-C bond is easier than the C-H bond. Hence, the main reaction of the C_3H_8 cracking is $C_3H_8 \rightarrow C_2H_5 + CH_3$, but not $C_3H_8 \rightarrow C_3H_7 + H$. Subsequently, the chain reactions can be transferred by both CH_3 and C_2H_5 radicals through the reactions $CH_3 + C_3H_8 \rightarrow C_3H_7 + CH_4$ and $C_2H_5 + C_3H_8 \rightarrow C_3H_7 + C_2H_6$, respectively.[22,24] However, the energy barrier of the former (11.5 kcal/mol) is a little lower than that of the latter (12.6 kcal/mol). This means that $CH_3 + C_3H_8 \rightarrow C_3H_7 + CH_4$ is the main reaction to consume C_3H_8 for generation of CH_4 and C_3H_7 radical, which can easily decompose to produce C_2H_4 and CH_3.[22] The CH_3 radicals will react with C_3H_8 again ($CH_3 + C_3H_8 \rightarrow C_3H_7 + CH_4$), resulting in transformation of C_3H_8 to CH_4 and C_2H_4.

Conclusion

We exploited a hybrid DBD plasma-thermal system for direct non-oxidative coupling of CH_4 to

C_2H_4 and H_2. The one-stage HPTSR shows high C_2H_4 selectivity of ca. 80 %, but CH_4 conversion is only 2 %. The two-stages HPTS (plasma stage followed by thermal stage), however, exhibits not only high C_2H_4 selectivity of ca. 63 %, but also a CH_4 conversion of ca. 17 %, suggesting an excellent potential for practical conversion of CH_4 to C_2H_4 and H_2. In addition, we will design highly efficient catalysts for stage 1 to selectively produce C_2H_6, and for stage 2 to manage C_2H_6 dehydrogenation, which may lead to an innovative, efficient and practical technique for non-oxidative coupling of CH_4 to C_2H_4 and H_2 without coking. Furthermore, although the current energy efficiency is very low, we believe there is significant room for further improvement by the synergy of catalysts with plasma and the high temperature. Based on the optimized reactor design and catalysts preparation, we are quite sure that it will achieve a high conversion/yield to offset cost increase caused by separating plasma and pyrolysis stages when scaling-up the process.

Declaration of Competing Interest

The authors declare that they have no known competing financial interests or personal relationships that could have appeared to influence the work reported in this paper.

Acknowledgment

This work was supported by the National Natural Science Foundation of China [22272015, 21503032], the Fundamental Research Funds for the Central Universities of China [DUT21JC40].

References

(1) Marks, T. J.; Arinaga, A. M.; Ziegelski, M. C. Alternative Oxidants for the Catalytic Oxidative Coupling of Methane. Angew. Chem. 132 (2020) 17935.

(2) Kim, I.; Lee, G.; Na, H. B.; Ha, J. M.; Jung, J. C. Selective Oxygen Species for the Oxidative Coupling of Methane. Mol. Catal. 435 (2017) 13−23.

(3) Galadima, A.; Muraza, O. Revisiting the Oxidative Coupling of Methane to Ethylene in the Golden Period of Shale Gas: A Review. J. Ind. Eng. Chem. 37 (2016) 1−13.

(4) Sarsani, S.; West, D.; Liang, W.; Balakotaiah, V., Autothermal Oxidative Coupling of Methane with Ambient Feed Temperature. Chemical Engineering Journal 328 (2017) 484-496.

(5) Xiaoguang Guo, Guangzong Fang, Gang Li, et al. Direct, nonoxidative conversion of methane to ethylene, aromatics, and hydrogen. *Science*, 344（2014) 616-619.

(6) David Bajec, Andrii Kostyniuk, Andrej Pohar, Blaž Likozar. Nonoxidative methane activation, coupling, and conversion to ethane, ethylene, and hydrogen over Fe/HZSM-5, Mo/HZSM-5, and Fe–Mo/HZSM-5 catalysts in packed bed reactor. *Int J Energy Res*. 43 (2019) 6852–6868.

(7) Yunfei Gao, Luke Neal, Dong Ding, et al. Gaffney, Fanxing Li. Recent Advances in Intensified Ethylene Production-A Review. *ACS Catal.* 9 (2019) 8592−8621.

(8) Tianyu Zhang. Recent advances in heterogeneous catalysis for the nonoxidative conversion of methane. *Chem. Sci.* 21 (2021) 12529–12545.

(9) X. Zhang, L. Di, Q. Zhou, Methane conversion under cold plasma over Pd-containing ionic liquids immobilized on γ-Al_2O_3, *J. Energy Chem*. 22 (2013) 446–450.

(10) Marco scapinello, Evangelos Delikonstantis, Georgios D. Stefanidis. The panorama of plasma-assisted non-oxidative methane reforming. *Chemical Engineering &Processing : Process Intensification*. 117 (2017) 120−140.

(11) Yang Xiao, Arvind Varma. Highly Selective Nonoxidative Coupling of Methane over Pt-Bi Bimetallic Catalysts. *ACS Catal*. 8 (2018) 2735-2740.

(12) Duygu Gerceker, Ali Hussain Motagamwala, Keishla R. Rivera-Dones, et al. Methane Conversion to Ethylene and Aromatics on PtSn Catalysts. *ACS Catal*. 7 (2017) 2088-2100.

(13) Lina Liu, Sonali Das, Zhikun Zhang, Sibudjing Kawi. Nonoxidative Coupling of Methane over Ceria-Supported Single-Atom Pt Catalysts in DBD Plasma. *Acs Appl. Mater. Interfaces.* 14 (2022) 5363-5375.

(14) Kim J, Jeoung J, Jeon J, et al. Effects of dielectric particles on non-oxidative coupling of methane in a dielectric barrier discharge plasma reactor. *Chem. Eng. J*. 377 (2019) 119896.

(15) Scapinello M, Delikonstantis E, Stefanidis G. D. A study on the reaction mechanism of non-oxidative methane coupling in a nanosecond pulsed discharge reactor using isotope analysis. *Chem. Eng. J*. 360 (2019) 64−74.

(16) Evangelos Delikonstantis, Marco Scapinello, Orelie Van Geenhoven, Georgios D. Stefanidis. Nanosecond pulsed discharge-driven non-oxidative methane coupling in a plate-to-plate electrode configuration plasma reactor. *Chem. Eng. J*. 380 (2020) 122477.

(17) Wang Kangjun, Li Xiaosong, Zhu Aimin. A Green Process for High-Concentration Ethylene and Hydrogen Production from Methane in a Plasma-Followed-by-Catalyst Reactor *Plasma Sci. Technol*. 13 (2011) 77.

(18) Kado S, Sekine Y, Urasaki K, Okazaki. K, Nozaki. T. High performance methane conversion into valuable products with spark discharge at room temperature. *Stud. Surf. Sci. Catal*. 147 (2004) 577-582.

(19) Shuiliang Yao, Akira Nakayama, Eiji Suzuki. Methane conversion using a high-frequency pulsed plasma: Important factors. *AlChE J.* 47 (2001) 413-418.

(20) Y. Yang. Direct Non-oxidative Methane Conversion byNon-thermal Plasma: Modeling Study. *Plasma Chem. Plasma Process.* 23 (2003) 327-346.

(21) C. De Bie, B. Verheyde, T. Martens, J.V.Dijk, S. Paulussen, A. Bogaerts. Fluid Modeling of the Conversion of Methane into Higher Hydrocarbons in an Atmospheric Pressure Dielectric Barrier Discharge. Plasma Process. Polym. 8 (2011) 1033-1058.

(22) K. M. Sundaram and G. F. Froment. Modeling of thermal cracking kinetics. 3. Radical mechanisms for the pyrolysis of simple paraffins, olefins, and their mixtures. Ind. Eng. Chem. Fundam. 17 (1978) 174-182.

(23) Pacey. P. D, Purnell. J. H. Thermodynamics of Simple Polar Liquids. Ind. Eng. Chem. Fundam. 11 (1972) 233-239.

(24) O.A. Stadnichenko, L. F. Nurislamova, N. S. Masyuk, VI. N. Snytnikov, and V. N. Snytnikov. Radical mechanism for the gas-phase thermal decomposition of propane. Reac Kinet Mech Cat. 123 (2018) 607-624.

Supporting Information

Additional supporting information may be found online in the Supporting Information section at the end of this article.

Supporting Information

Hybrid Plasma-Thermal System for Methane Conversion to Ethylene and Hydrogen

Rui Liu [1], Yingzi Hao [1], Tong Wang [1], Li Wang [2], Annemie Bogaerts [3], Hongchen Guo*[1], and Yanhui Yi*[1]

[1] State Key Laboratory of Fine Chemicals, School of Chemical Engineering, Dalian University of Technology, Dalian 116024, P.R. China.

[2] College of Environmental Sciences and Engineering, Dalian Maritime University, Dalian 116026, Liaoning, China.

[3] Research group PLASMANT, Department of Chemistry, University of Antwerp, Universiteitsplein 1, BE-2610 Wilrijk-Antwerp, Belgium.

List of contents

1. Thermodynamic calculation of CH_4 pyrolysis

2. Experimental section

3. Method of measure the temperature in one-stage HPTS

4. Discharge parameters in one-stage HPTS

5. Plasma pyrolysis of CH_4 in DBD

6. H_2 selectivity in one-stage HPTS

7. Thermal pyrolysis of CH_4

8. Effect of SEI in one-stage HPTS

9. Effect of flow rate in one-stage HPTS

10. Relationship of temperature and SEI in stage 1 of two-stage HPTS

11. Effect of flow rate in two-stage HPTS

12. Effect of the coke in two-stage HPTS

13. Effect of distance in two-stage HPTS

14. Compared with the energy consumption in different system.

15. Thermal pyrolysis of C_2H_6

16.Thermal pyrolysis of C_3H_8

17.Thermal pyrolysis of C_4H_{10}

18. Literature Cited

Table S1 Some catalytic results of the methane non-oxidation coupling reactions

Table S2 Catalytic performance of ethane dehydrogenation.

Table S3 Catalytic performance of propane dehydrogenation.

Table S4 The main reaction Scheme for the Pyrolysis of ethane.

Table S5 The main reaction Scheme for the Pyrolysis of propane.

Figure S1. Thermodynamic equilibrium calculation of CH_4 pyrolysis, including CH_4 conversion (right y-axis) and product selectivity (left y-axis; C-based for C_2H_6, C_2H_4 and C_2H_2; and H-based for H_2).
Figure S2. Schematic diagrams of the setup for one-stage hybrid plasma-thermal system (a) and two-stage hybrid plasma-thermal system (b) for CH_4 to C_2H_4 conversion.
Figure S3. schematic diagram of One-Stage hybrid plasma-thermal system.
Figure S4. The temperature measured by infrared thermometer.
Figure S5. The real-time temperature from thermocouple and infrared thermometer varies the setting temperature of furnace.
Figure S6. (a) Discharge voltages, (b) discharge currents and (c) Lissajous plots in the one-stage hybrid plasma-thermal system, with varying temperature adjusted by external heating.
Figure S7. Experimental results of CH_4 pyrolysis by DBD plasma as a function of SEI, without external heating, at a temperature of ca. 180℃ to 400℃.
Figure S8. H_2 selectivity as a function of temperature in one-stage HPTS.
Figure S9. Experimental results of thermal pyrolysis of CH_4.
Figure S10. CH_4 conversion and product selectivity in one-stage HPTS, as a function of SEI adjusted by applying different voltages.
Figure S11. Reaction performance of one-stage HPTS for methane to ethylene conversion with different flow rates. (a) CH_4 conversion and C_2H_4 selectivity as a function of temperature; (b) CH_4 conversion and C_2H_4 selectivity as a function of SEI; (c) CH_4 conversion versus C_2H_4 selectivity.
Figure S12. Effect of SEI on temperature in stage 1 of two-stage HPTS
Figure S13. CH_4 conversion (a) and C_2H_4 selectivity (b) as a function of temperature in two-stage HPTS
Fgure S14.The coke on the surface of the electrode (a) and the CH_4 conversion (b) with time on stream.
Figure S15. CH_4 conversion and product selectivity in two-stage HPTS, as a function of the distance between stage 1 and stage 2.
Figure S16. Energy consumption with methane feed flow rate of different reaction system (a); comparison of energy consumption and energy efficiency of different methane feed flow rate.
Figure S17. Reaction results of thermal pyrolysis of C_2H_6 in stage 2.
Figure S18. Reaction results of thermal pyrolysis of C_3H_8 in stage 2.
Figure S19. Reaction results of thermal pyrolysis of i-C_4H_{10} in stage 2.

Table S1 Some catalytic results of the methane non-oxidation coupling reactions [a]

Year	Catalysts	Reaction conditions			Conversion	Selectivity (%)			References
		Reactants	pressure	Temperature		C_2H_6	C_2H_4	C_2H_2	
1999	0.4%Ni-Ti	Pure CH_4	10 atm	450℃	20%	22%	55%	-	1[b]
2008	$(\equiv SiO)_2Ta$-H	Pure CH_4	50 atm	below 500℃	0.5%	98%	-	-	2-
2011	PtH-MFI	Pure CH_4	1 atm	370℃	0.15%	95%	-	-	3
2014	Fe@SiO_2	CH_4/N_2=9/1	1 atm	1090℃	48.1%	-	48.4%	-	4
2016	Fe©SiO_2	diluted CH_4	1 atm	1030℃	20%	65%			5
2017	PtSn/H-ZSM-5	Pure CH_4	1 atm	700℃	0.06%	-	>95%	-	6
2017	In/SiO_2	Pure CH_4	1 atm	825℃	<1%	86%		-	7
2018	Pt_1@CeO_2	CH_4/He=1/99	1 atm	975℃	14.4%	74.6%			8-
2018	Mo_2C[B]ZSM-5	CH_4/He=5/95	1 atm	650℃	1%		>90%		9
2018	Pt-Bi/zeolite	CH_4/N_2 = 1/9	0.1 atm	600-700℃	2-3%	90%	-	-	10
2019	Fe–Mo/HZSM-5	CH_4/N_2=9/1	1.5 atm	700℃	2 %	23%	36%	-	11
2019	Fe©CRS	CH_4/H_2=1/1	1 atm	1080℃	5.8-6.9%	86.2%			12-
2019	Fe/SiO_2	CH_4/N_2=9/1	1 atm	1000℃	12%	<35%		-	13
2020	GaN/SBA15	CH_4/A_r=5/1	1atm	750℃	0.32%	-	71%	-	14
2020	Ni-P/SiO_2	Pure CH_4	1 atm	850℃	0.08%	99.9%		-	15
2020	Pt@CeO_2	diluted CH_4	1.5 atm	780-910℃	4.3%	60%			16
2020	Ta^8O+	-	-	-	-	main	-	-	17
2020	Fe^{II}/SiO_2	Pure CH_4	-	1080℃	3-4%	20%			18
2021	Fe-reactor	CH_4/N_2=9/1	1 atm	1000℃	7.3%	41.2%			19

[a] only the methane non-oxidation coupling conversion to C_2 products.
[b] CH_4 was recycled to be converted continuously for 22 h, and the produced H_2 was separated from reaction system to shift the reaction equilibrium.

Table S2 .Catalytic performance of ethane dehydrogenation.

Catalyst	Temperature (℃)	Conversion (%)	Selectivity (%)	Reference
Pt-Sn/MgO	600	3	100	26
Pt-In/SiO_2	600	15	99	27
Au/SiO_2	650	16	95	28
Ni-Ga/Al_2O_3	600	10	94	28
Cr_2O_3/SiO_2	650	19	98	29
Ga_2O_3/Al_2O_3	650	28	93	30
Fe/ZSM-5	600	22	72	31

Table S3 .Catalytic performance of propane dehydrogenation.

Catalyst	Temperature (℃)	Conversion (%)	Selectivity (%)	Reference
Pt_3-Mn/SiO_2	550	6.8	95	32
Pt-Cu/h-BN	600	24	97	33
Pt/In/Mg(Al)O_x	620	69	98	34
K-$CrZr_5O_x$	550	54	95	35
GrO_x/Al_2O_3	600	33	90	36
Ce-CrOx/ Al_2O_3	630	86	78	37

Table S4. The main reaction Scheme for the Pyrolysis of ethane.[38]

No.	Reaction	A, S^{-1} or L mol^{-1} S^{-1}	E, kcal/mol
1	$C_2H_6 \rightarrow 2CH_3\cdot$	4.0×10^{16}	87.5
2	$C_2H_6 + CH_3\cdot \rightarrow C_2H_5\cdot + CH_4$	3.8×10^{11}	16.5
3	$C_2H_5\cdot \rightarrow C_2H_4 + H\cdot$	3.2×10^{13}	40
4	$C_2H_6 + H\cdot \rightarrow C_2H_5\cdot + H_2$	1.0×10^{11}	9.7
5	$CH_3\cdot + CH_3\cdot \rightarrow C_2H_6$	1.3×10^{10}	0
6	$C_2H_5\cdot + CH_3\cdot \rightarrow C_3H_8$	3.2×10^{9}	0
7	$C_2H_5\cdot + C_2H_5\cdot \rightarrow C_2H_6 + C_2H_4$	5.0×10^{7}	0

Table S5. The main reaction Scheme for the Pyrolysis of propane.[38]

No.	Reaction	A, S^{-1} or L mol^{-1} S^{-1}	E, kcal/mol
1	$C_3H_8 \rightarrow C_2H_5\cdot + CH_3\cdot$	2.0×10^{16}	84.5
2	$C_3H_8 + CH_3\cdot \rightarrow 1\text{-}C_3H_7\cdot + CH_4$	3.4×10^{10}	11.5
3	$C_3H_8 + CH_3\cdot \rightarrow 2\text{-}C_3H_7\cdot + CH_4$	4.0×10^{9}	10.1
4	$C_3H_8 + C_2H_5\cdot \rightarrow 1\text{-}C_3H_7\cdot + C_2H_6$	1.2×10^{9}	12.6
5	$C_3H_8 + C_2H_5\cdot \rightarrow 2\text{-}C_3H_7\cdot + C_2H_6$	8.0×10^{8}	10.4
6	$1\text{-}C_3H_7\cdot \rightarrow C_2H_4 + CH_3\cdot$	4.0×10^{13}	32.6
7	$1\text{-}C_3H_7\cdot \rightarrow C_3H_6 + H\cdot$	2.0×10^{13}	38.4
8	$2\text{-}C_3H_7\cdot \rightarrow C_3H_6 + H\cdot$	2.0×10^{13}	38.7

1. Thermodynamic calculation of CH_4 pyrolysis

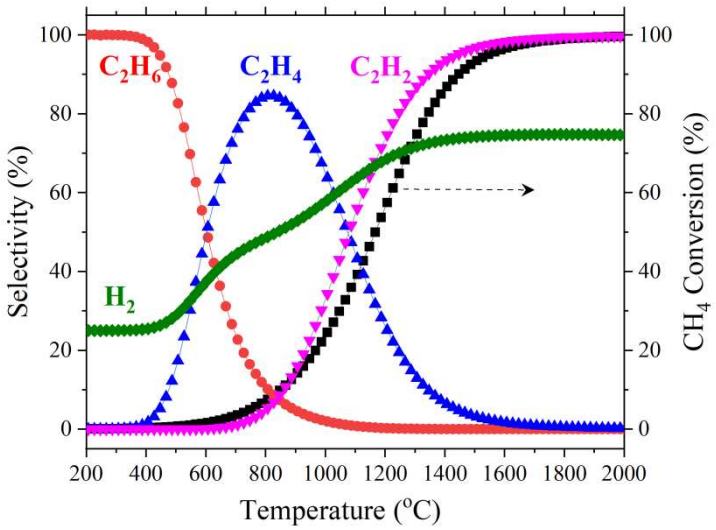

Figure S1. Thermodynamic equilibrium calculation of CH_4 pyrolysis, including CH_4 conversion (right y-axis) and product selectivity (left y-axis; C-based for C_2H_6, C_2H_4 and C_2H_2; and H-based for H_2).

The equilibrium composition was obtained based on the thermodynamic analysis method (database system of TheCoufal) adopted from literature.[20] In this thermodynamic calculation, the products of coke and aromatic hydrocarbons were not included, aiming to concise the trend of C_2 hydrocarbons selectivity. The selectivity of C_2H_6, C_2H_4 and C_2H_2 is based on the carbon balance, while the selectivity of H_2 is based on the hydrogen balance.

It can be seen from Figure S1 that at a temperature below 500 °C, C_2H_6 is the dominant product with nearly 100 % selectivity. With temperature increasing from 500 °C up to 800 °C, C_2H_4 becomes the main product at 600 °C, and the dominant product at 800 °C, with selectivity more than 80%. With temperature further increasing, the selectivity of C_2H_4 gradually decreases, while the selectivity of C_2H_2 gradually increases, and C_2H_2 becomes the main product at 1080 °C. For temperatures higher than 1400 °C, C_2H_2 becomes the dominant product with selectivity more than 90%. However, significant CH_4 conversion can be obtained only when the temperature is higher than 800 °C.

2. Experimental section

2.1 Experimental setup

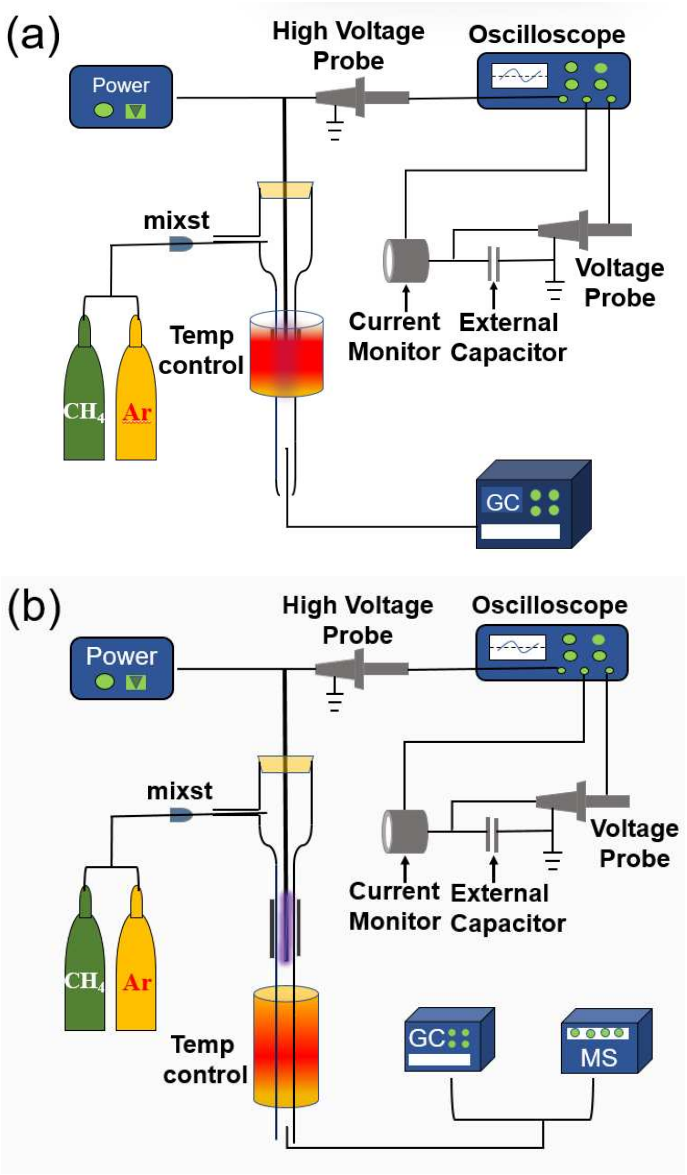

Figure S2. Schematic diagrams of the setup for one-stage hybrid plasma-thermal system (a) and two-stage hybrid plasma-thermal system (b) for CH_4 to C_2H_4 conversion.

All experiments were carried out in a tubular quartz reactor. The inner diameter of the quartz reactor were 8 mm. A Fe-Cr-Al wire served as the ground electrode by wrapping around the reactor. A stainless-steel rod with diameter of 2 mm was used as a high-voltage electrode. The discharge zone in the reactor was 80 mm long and the discharge gap was 3 mm. The bulk reaction temperature was controlled from 200 to 880℃ by a furnace. In the hybrid system, we controlled the temperature by manually increasing

the furnace temperature with a ramp (20 °C or 50 °C). In the plasma only system without external heating, we controlled the temperature by changing the discharge power. The only difference in one-stage HPTS (Figure S2a) and two-stage HPTS (Figure S2b) is that the DBD plasma and the external heating were spatially together or not. In two-stage HPTS, the heater for stage 2 placed on the same quartz tube as plasma stage 1 and the isothermal zone of stage 2 was 100 mm. Typically, the flow rate of the feedstock was 20 mL/min (CH_4: Ar = 1:1), which was controlled by two gas controllers. Argon is added for the purpose for enlarging the discharge and avoiding too much coking. A sinusoidal AC power supply (Suman, CTP-2000K) was connected with a transformer. The initial power and the frequency of the DBD plasma were fixed at 25 W and 14.1 kHz, respectively. The discharge parameters were collected by a digital phosphor oscilloscope (Tektronix, DPO 3012). The applied voltage of the plasma reactor was measured by a high voltage probe (1000:1, P6015A, Tektronix). The voltage across the 0.1 μF capacitor was measured by a voltage probe (10:1, TPP0101, Tektronix), which connected with the two sides of the capacitor. A current probe (Pearson 6585) was connected on the ground electrode to evaluate the current across the DBD plasma reactor. The exhaust gas is analyzed online by a mass spectrometer (HIDEN DECRA) with the Faraday detection mode, which was mainly used to make a qualitative analysis for the variation of products at three stages (plasma only, thermal cracking only and hybrid plasma-thermal system). All experiments were operated at atmospheric pressure.

2.2 Conversion, product analysis, energy consumption and energy efficiency

The effluent gases after the hybrid system reactor were analyzed by an online gas chromatograph (Tianmei GC7900), which was equipped with FID detector and PLOT column (Al_2O3, 50m × 0.53mm × 25μm). The GC was mainly used to make a quantitative analysis for the effluent gases (CH_4, C_2H_2, C_2H_4, C_2H_6, C_3H_6, C_3H_8, i-C_4H_8, and n-C_4H_{10}) after the hybrid system reactor. The concentrations of each species were calculated using an external standard method with standard curves obtained from calibrated gas mixtures. It is mentioned that the products includes other carbonaceous in the only plasma discharge or Plasma-thermal hybrid system with a low external heating temperature, but the C_5+ products were very little. Hence, we subsumed the C_5+ products into the coke. However, in the Plasma-thermal hybrid system

(> 600 °C), there was no more products have been monitored expect our reports. It can be attributed that the majority of high carbon hydrocarbon have been cleaved at a higher temperature. The selectivity of the gas-phase products and coke are calculated based on the following equations.

$$\text{Conversion of } CH_4\ (\%) = \frac{\text{Moles of } CH_4 \text{ converted}}{\text{Moles of } CH_4 \text{ input}} \times 100\%$$

$$\text{Selectivity of } C_xH_y\ (\%) = \frac{\text{Moles of } C_xH_y \text{ produced} \times x}{\text{Moles of } CH_4 \text{ converted}} \times 100\%$$

$$\text{Selectivity of } H_2\ (\%) = \frac{\text{Moles of } H_2 \text{ produced} \times 0.5}{\text{Moles of } CH_4 \text{ converted}} \times 100\%$$

$$\text{Selectivity of coke } (\%) = 1 - \sum_{x=2}^{x=4} \text{selectivity of } C_xH_y$$

The specific energy input (SEI) is calculated using the following equation, where P(W) is the input power, F(ml/min) is the flow rate of the feed gas, and 60 is the conversion from minutes to seconds.

$$SEI(kJ/L) = 60 \times \frac{P(W)}{F(ml/min)}$$

The specific energy requirement (SER) is the energy required for full conversion of one CH_4 mole and is expressed as:

$$SER(kJ/mol) = \frac{SEI}{Conversion}$$

The energy consumption (EC) is the energy required for the main product, and is expressed as:

$$EC\ (kJ\ mol^{-1}) = 2 \times SEI / (Conversion \times Main\ product\ Selectivity)\ [kJ\ mol^{-1}]$$

The Energy efficiency (η, in %) is expressed as:

$$\eta\ (\%) = 100 \times \Delta H_r^{\ominus} / SER$$

Where $\Delta H_r^{\ominus}$ is the enthalpy of the CH_4 coupling reaction, which is taken as a function of temperature: $\Delta H_r(880°C)$=251.1 kJ/mol, $\Delta H_r(20°C)$=201.5 kJ/mol, and $\Delta H_r(180°C)$=207.6 kJ/mol, and EC is also expressed in kJ/mol.

3. Method of measure the temperature in Stage-one HPTS

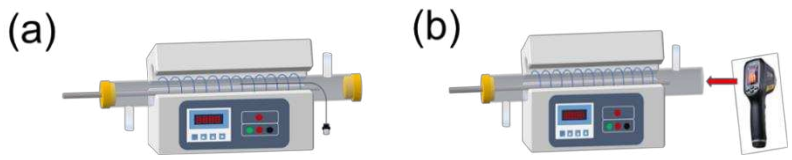

Figure S3. Schematic diagram of One-Stage hybrid plasma-thermal system.

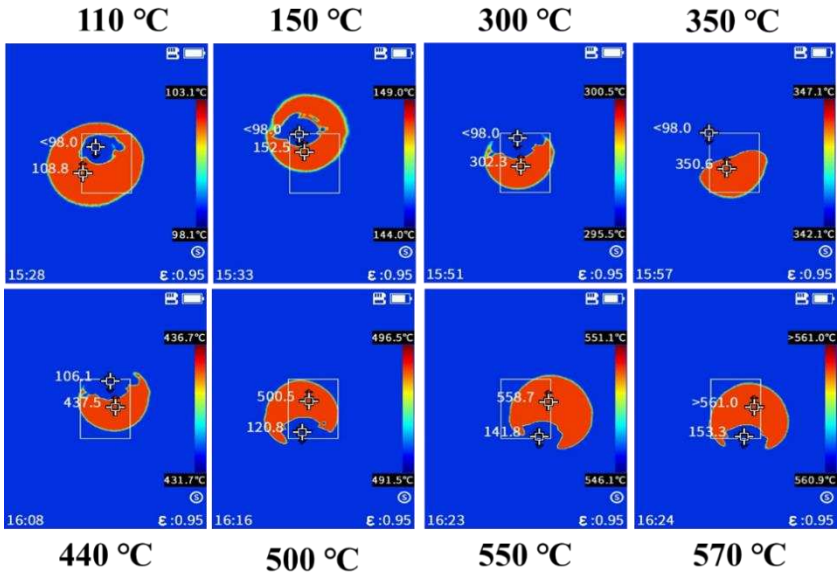

Figure S4. The temperature measured by infrared thermometer.

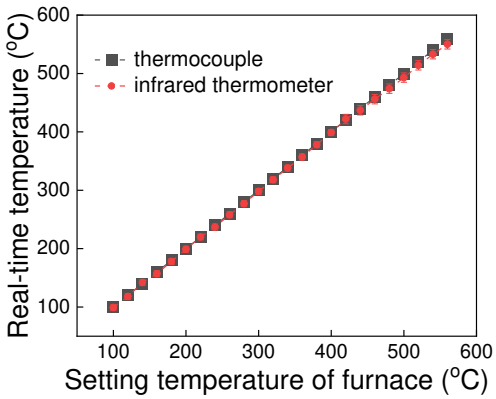

Figure S5. The real-time temperature from thermocouple and infrared thermometer varies with the setting temperature of furnace.

4. Discharge parameters in one-stage HPTS

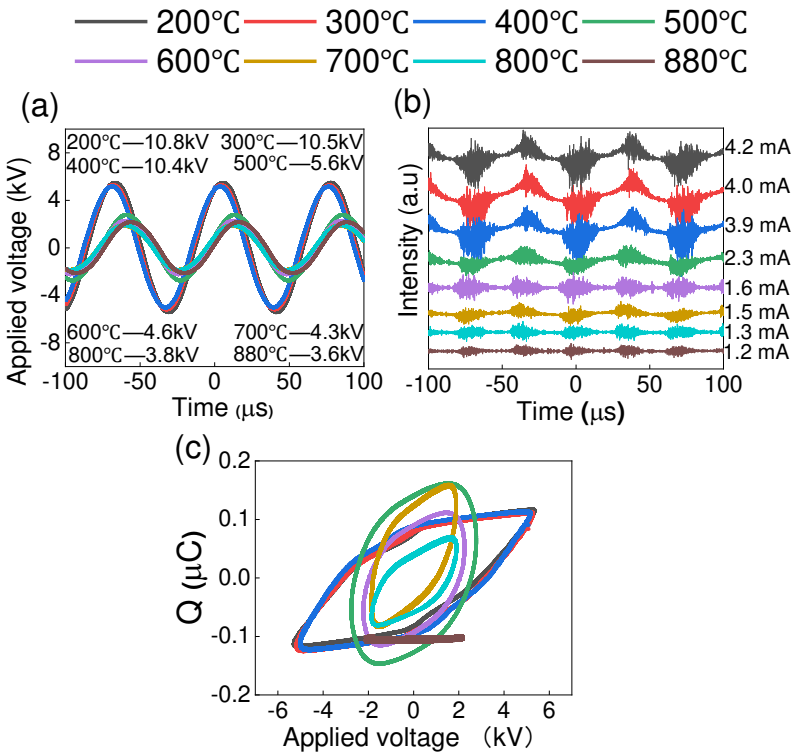

Figure S6. (a) Discharge voltages, (b) discharge currents and (c) Lissajous plots in the one-stage hybrid plasma-thermal system, with varying temperature adjusted by external heating.

Usually, the electron density in the plasma is proportional to the discharge current. The number of micro-discharges decreases with increasing temperature (Figure S6b). Therefore, the discharge current decreases with increasing temperature, which means that the electron density in the DBD plasma gradually reduces with increasing temperature. Thus, a smaller number of electrons will give rise to electron impact dissociation of CH_4, resulting in a lower CH_4 conversion. Additionally, the peak-peak of discharge voltage decreases with increasing temperature (Figure S3a), which means a weaker electric field was obtained at a higher temperature (E=U/d). The reduced electron density and electric field caused a lower probability of C-H bond dissociation and thus suppressed the CH_4 conversion at elevated temperature. In Figure S3c, with increasing temperature, the areas of the Lissajous figures gradually decreases, which indicates that the input power reduces. In summary, in the one-stage HPTS, the input power decreases with increasing the temperature.

5. Plasma pyrolysis of CH_4 in DBD without external heating

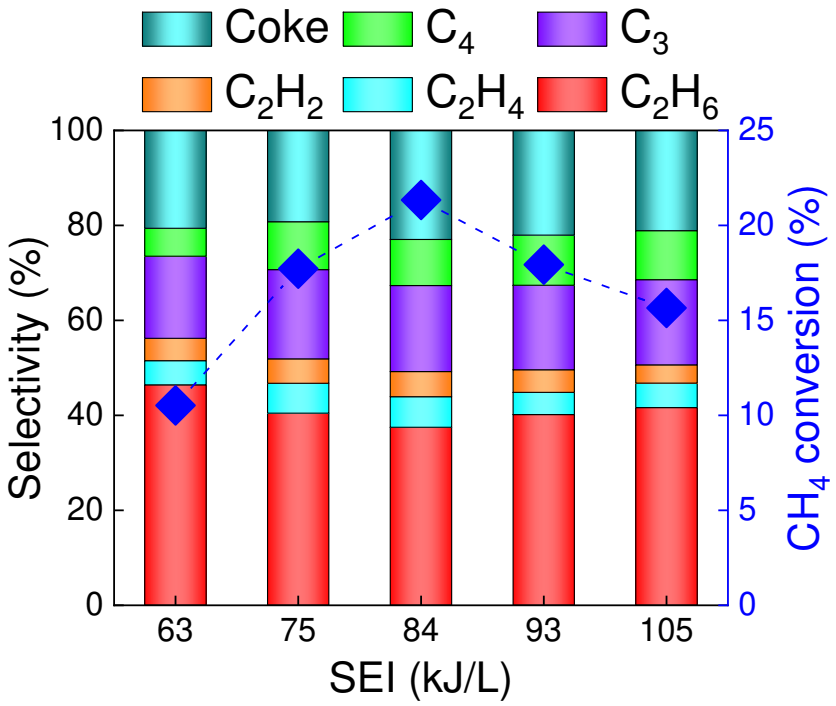

Figure S7. Experimental results of CH_4 pyrolysis by DBD plasma as a function of SEI, without external heating, at a temperature of ca. 180℃ to 400℃.

In Figure S7, the CH_4 conversion and product selectivities are plotted as a function of SEI applied to the discharge without external heating. At a constant flow rate of 20 ml/min, increasing SEI means higher input power.[21] Figure S4 shows that, in case of plasma only, the CH_4 conversion increases with rising SEI up to 84 kJ/L, but the selectivity towards C_2H_6 significantly drops. The same trend in the selectivity changes was found in previous studies.[22,23] However, different from previous reports,[24] as the SEI increases above 84 kJ/L, the CH_4 conversion drops. This may be caused by the accumulation of carbon, which inhibits the discharge and thus suppresses the dissociation and activation of CH_4. Importantly, C_2H_6 is clearly the dominant product, while C_2H_4 and also C_2H_2 are only formed in minor amounts.

6. H_2 selectivity in one-stage HPTS

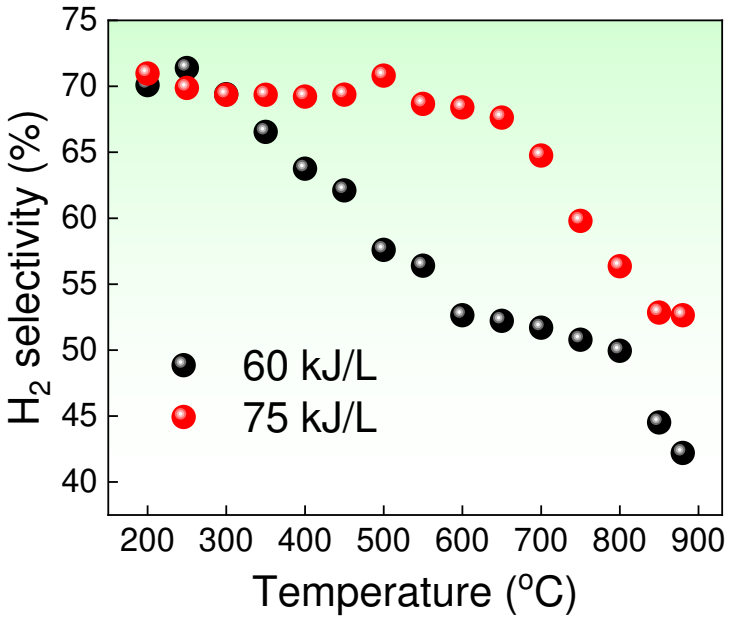

Figure S8. H_2 selectivity as a function of temperature in one-stage HPTS.

7. Thermal pyrolysis of CH_4

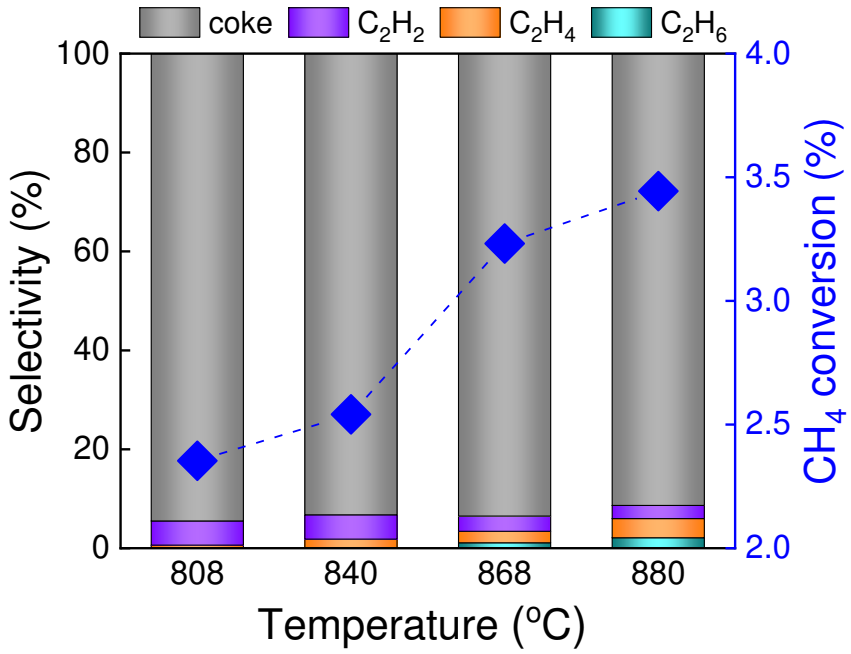

Figure S9. Experimental results of thermal pyrolysis of CH_4.

In Figure S9, a thermal pyrolysis of CH_4 experiment showed a CH_4 conversion of 2-3.5%, and around 97% of the product was coke. The conversion of CH_4 decreases and the the selectivity of C_2 increases with increasing the temperature.

8. Effect of SEI in one-stage HPTS

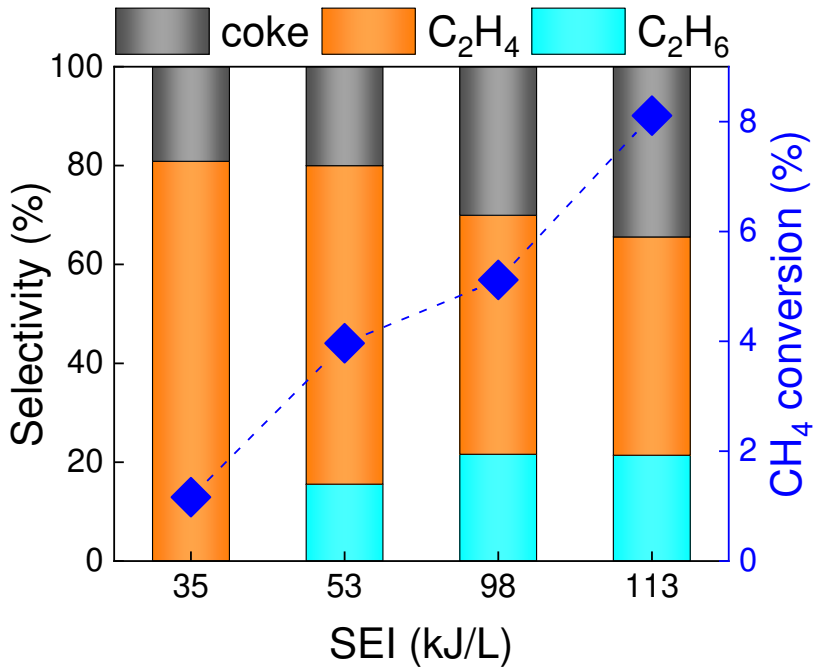

Figure S10. CH_4 conversion and product selectivity in one-stage HPTS, as a function of SEI adjusted by applying different voltages.

Figure S10 shows that the CH_4 conversion and C_2H_6 selectivity sightly increase, while the C_2H_4 selectivity decreases with increasing SEI at 880 °C. It was also confirmed that the CH_4 conversion is inversely proportional to the selectivity of C_2 products with general applicability in the one-stage HPTS. That is, it is needed to establish a new reaction system.

9. Effect of flow rate in one-stage HPTS

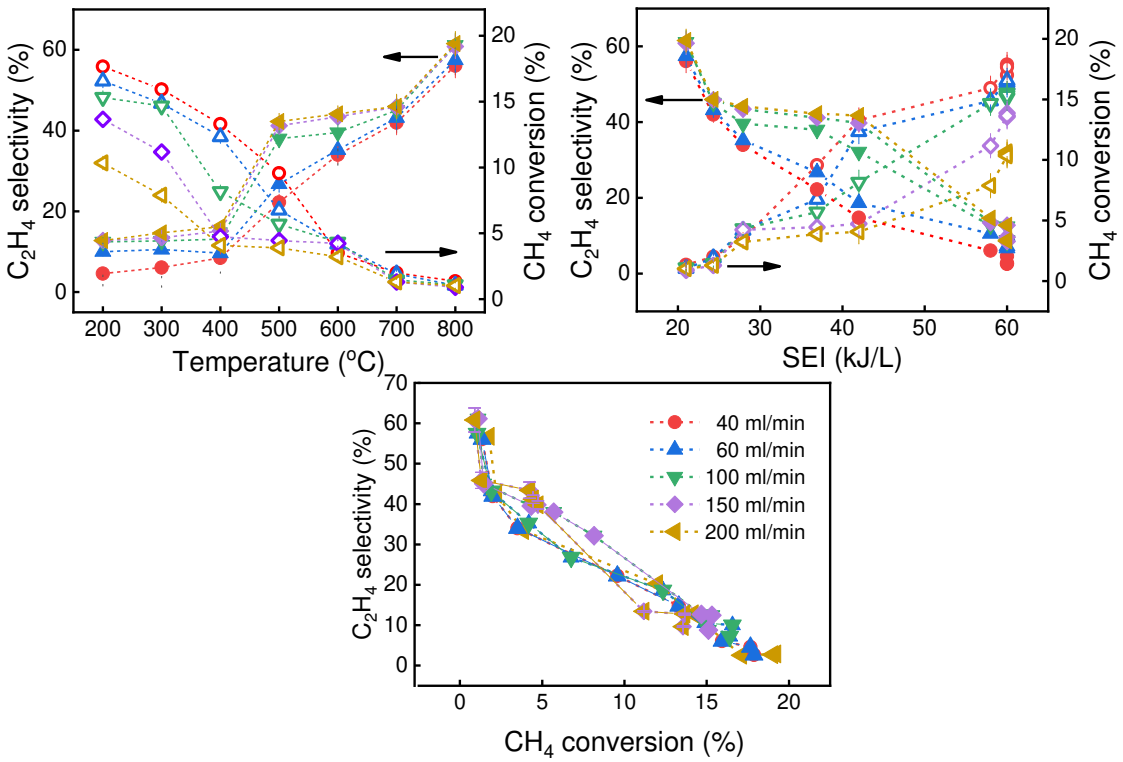

Figure S11. Reaction performance of one-stage HPTS for methane to ethylene conversion with different flow rates. (a) CH_4 conversion and C_2H_4 selectivity as a function of temperature; (b) CH_4 conversion and C_2H_4 selectivity as a function of SEI; (c) CH_4 conversion versus C_2H_4 selectivity.

Figure S11 shows the performance of one-stage HPTS for different flow rates. Upon increasing the external temperature, the SEI decreases, which leads to a lower CH_4 conversion but a higher C_2H_4 selectivity (Figure S11a and 11b). That is, the trade-off relationship between CH_4 conversion and C_2H_4 selectivity applies to the one-stage HPTS for methane to ethylene conversion at all the flow rates investigated (Figure S11c).

10. Relationship of temperature and SEI in stage 1 of two-stage HPTS

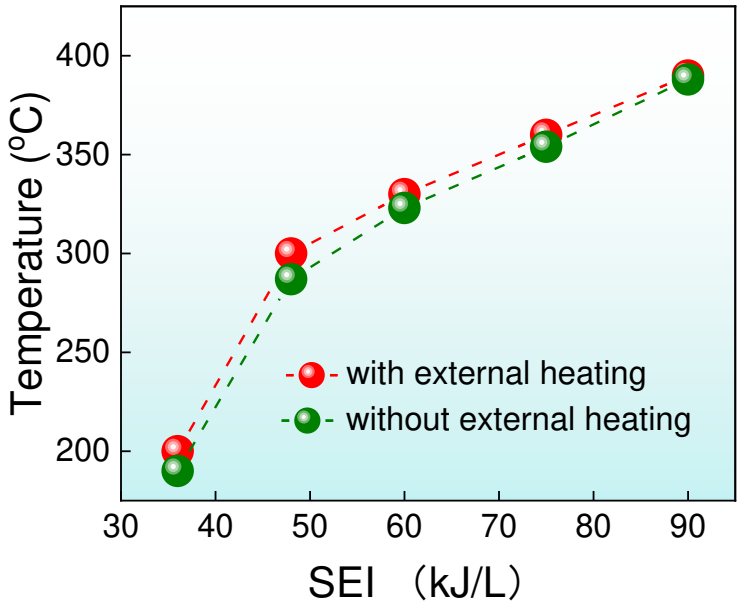

Figure S12. Effect of SEI on temperature in stage 1 of two-stage HPTS

In two-stage HPTS, the temperature of stage 1 was enhanced with increasing the SEI. The temperature of DBD reactor (stage 1) without external heating is a little lower than that with external heating. In theory, the CH_4 conversion increases with increasing the SEI of the stage 1. However, in experiment, the DBD discharge will be on fire with continuously increasing SEI in our setup.

11. Effect of flow rate in two-stage HPTS

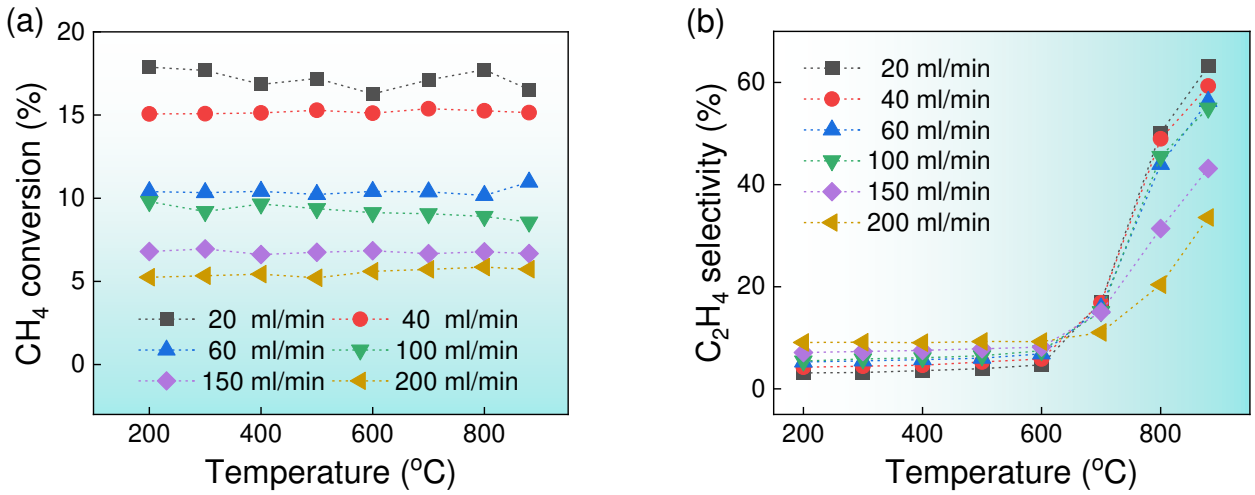

Figure S13. CH_4 conversion (a) and C_2H_4 selectivity (b) as a function of temperature in two-stage HPTS

12. Effect of the coke in two-stage HPTS

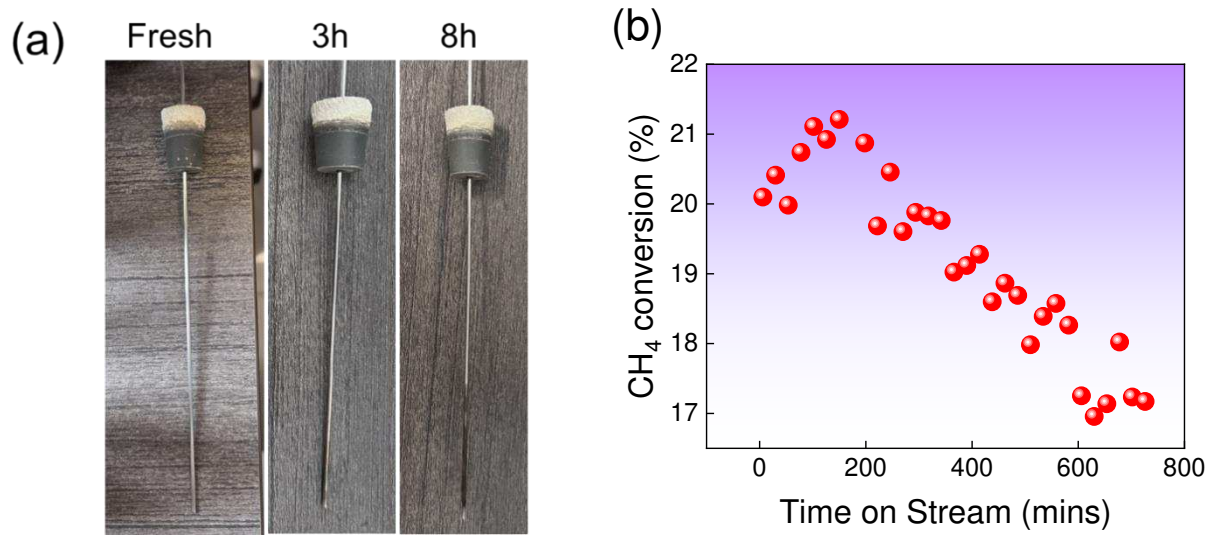

Fgure S14.The coke on the surface of the electrode (a) and the CH_4 conversion (b) varies with time on stream.

The CH_4 conversion decreases with the time on stream due to the accumulation of coke.

13. Effect of distance in two-stage HPTS

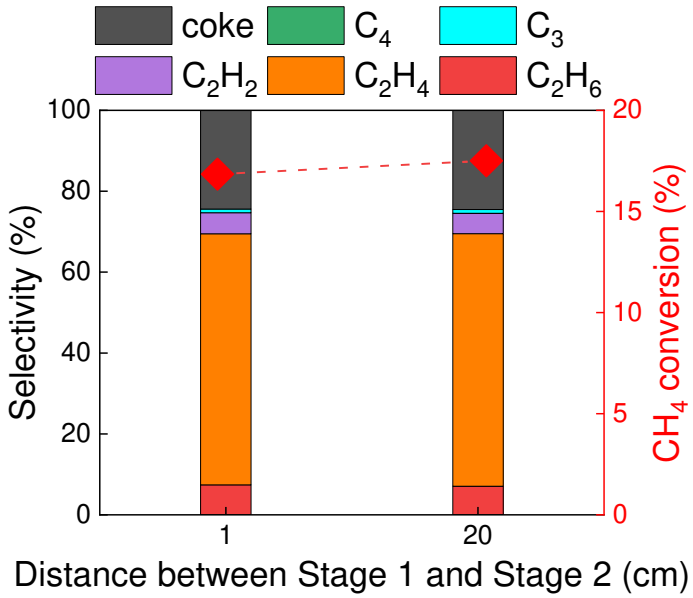

Figure S15. CH_4 conversion and product selectivity in two-stage HPTS, as a function of the distance between stage 1 and stage 2.

Figure S15 shows the effect of distance between the DBD (stage 1) and the thermal pyrolysis (stage 2) on reaction performance. However, no obvious effects were found when the distance varied from 1 cm to 20 cm.

14. Compared with the energy consumption in different system.

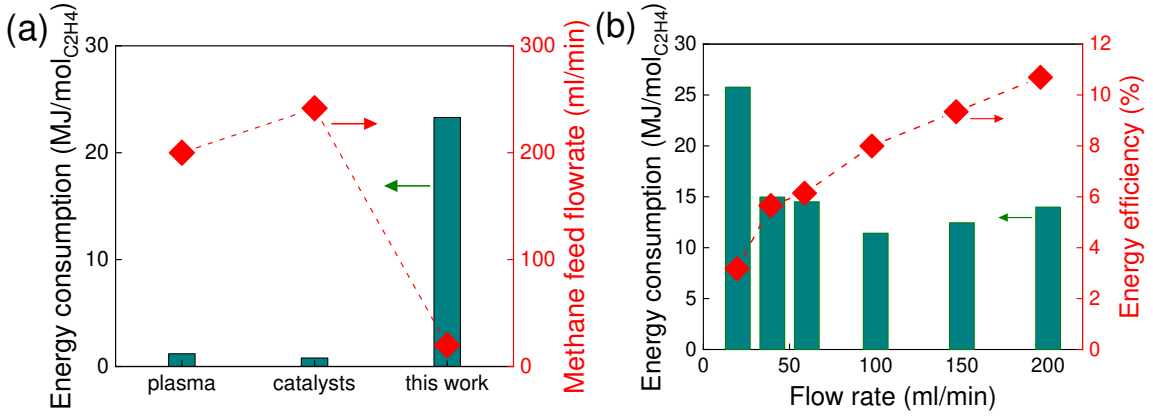

Figure S16. Comparison of energy consumption with the best results in literature using plasma or catalysts (a); energy consumption and energy efficiency in this two-stages HPTS with varied CH_4 flow rate (b).

$$EC(kJ/mol) = \frac{2\times1345\times P(W)}{F(ml/min)\times Methane\ conversion\times Main\ product\ selectivity} \quad (1)$$

$$\eta(\%) = \frac{100\times\Delta H_r^{\ominus}\times F(ml/min)\times Methane\ conversion}{1345\times P(W)} \quad (2)$$

Figure S16 a shows the energy consumption of plasma (1.2 MJ/mol),[25] traditional catalysis (0.8 MJ/mol),[4] and our two-stage HPTS (24.4 MJ/mol).Figure S16 b shows the effect of CH_4 flow rate on energy consumption and energy efficiency in the two stages HPTS. It can be find that energy consumption dramatically decreased, but energy efficiency obviously increased, with increasing CH_4 flow rate.

15. Thermal pyrolysis of C_2H_6

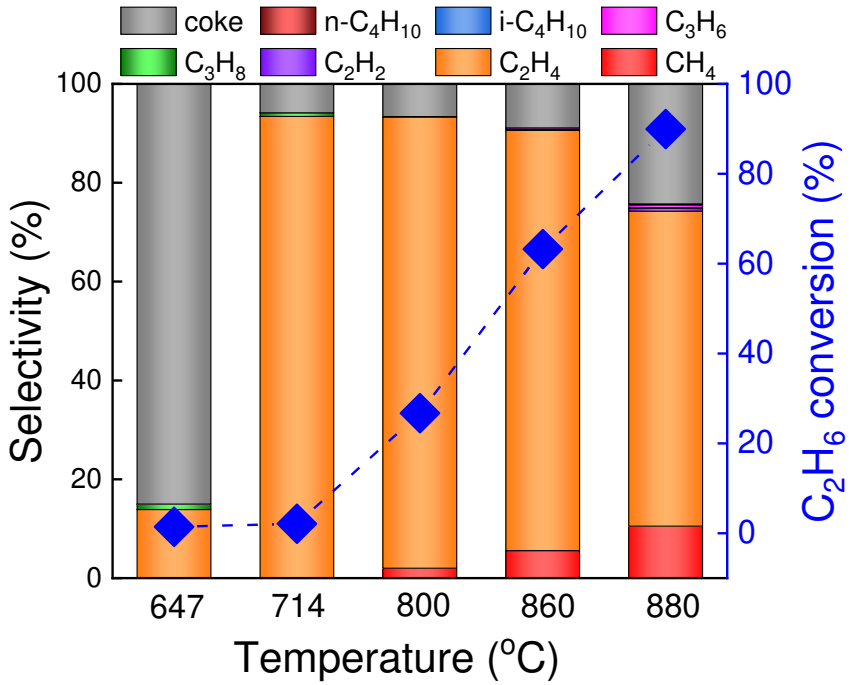

Figure S17. Reaction results of thermal pyrolysis of C_2H_6 in stage 2.

The main product of C_2H_6 dehydrogenation is C_2H_4. Some literature have reported the ethane pyrolysis, in which reaction temperatue is lower than ours (800 °C) because the catalyst has been used in these reports, as shown in Table S2.

16.Thermal pyrolysis of C_3H_8

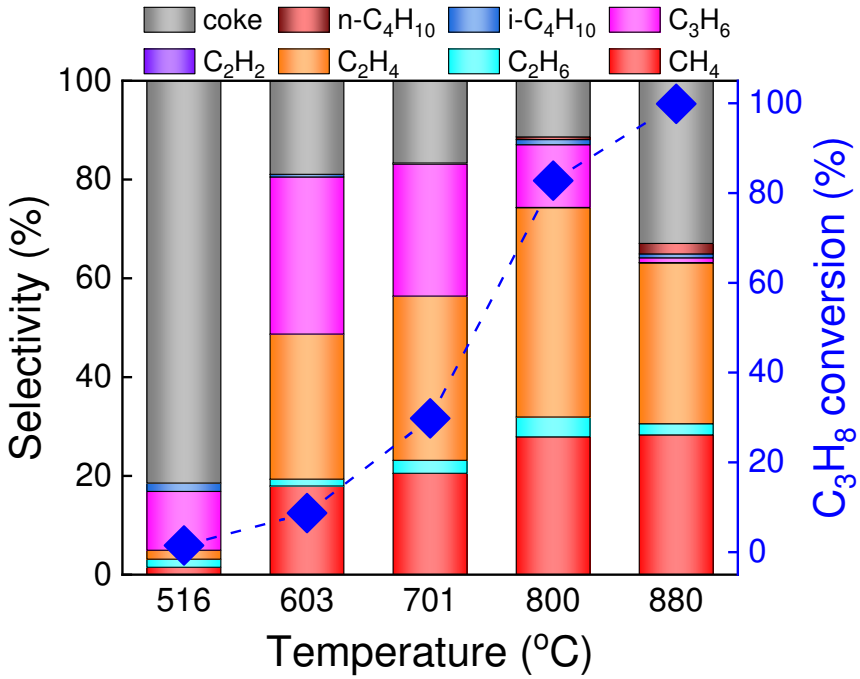

Figure S18. Reaction results of thermal pyrolysis of C_3H_8 in stage 2.

The main product of C_3H_8 dehydrogenation is from C_3H_6 to C_2H_4 with increasing the temperature. Some literature have reported the propane pyrolysis with a lower temperature because the catalyst has been used in these reports, as shown in Table S3.

17.Thermal pyrolysis of C_4H_{10}

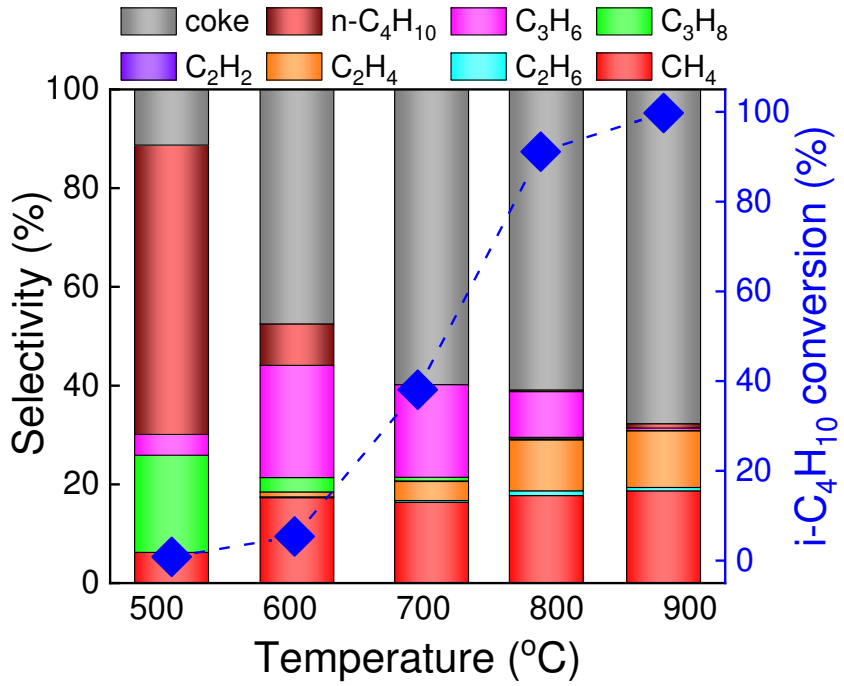

Figure S19. Reaction results of thermal pyrolysis of i-C_4H_{10} in stage 2.

18. Literature Cited

[1] M. V. Tsodikov, Ye. V. Slivinskii, V. P. Mordovin, O. V. Bukhtenko, G. Colón, M. C. Hidalgo and J. A. Navío. Low temperature selective methane activation to alkenes by a new hydrogen-accumulating system. *Chem. Commun*. **1999**, 943–944.

[2] Daravong Soulivong, Se´bastien Norsic, Mostafa Taoufik, Christophe Cope´ret, Jean Thivolle-Cazat, Sudhakar Chakka, and Jean-Marie Basset. Non-Oxidative Coupling Reaction of Methane to Ethane and Hydrogen Catalyzed by the Silica-Supported Tantalum Hydride: $(\equiv SiO)_2Ta\text{-}H$. *J. Am. Chem. Soc.* **2008**, 130, 5044–5045.

[3] Dmitry B. Lukyanov, Tanya Vazhnova. Transformation of methane over platinum supported catalysts at moderate temperature. *Journal of Molecular Catalysis A: Chemical*. **2011**. 342–343.

[4] Xiaoguang Guo, Guangzong Fang, Gang Li, Hao Ma, Hongjun Fan, Liang Yu, Chao Ma, Xing Wu, Dehui Deng, Mingming Wei, Dali Tan, Rui Si, Shuo Zhang, Jianqi Li, Litao Sun, Zichao Tang, Xiulian Pan, Xinhe Bao. Direct, Nonoxidative Conversion of Methane to Ethylene, Aromatics, and Hydrogen. *Science,* **2014**, 344, 616-619.

[5] Mann Sakbodin, Yiqing Wu, Su Cheun Oh, Eric D. Wachsman, and Dongxia Liu. Hydrogen-Permeable Tubular Membrane Reactor: Promoting Conversion and Product Selectivity for Non-Oxidative Activation of Methane over an Fe©SiO2 Catalyst. *Angew. Chem*. **2016**, 128, 16383 –16386.

[6] Duygu Gerceker, Ali Hussain Motagamwala, Keishla R. Rivera-Dones, James B. Miller, George W. Huber, Manos Mavrikakis, and James A. Dumesic. Methane Conversion to Ethylene and Aromatics on PtSn Catalysts. *ACS Catal.* **2017**, 7, 2088−2100.

[7] Yuta Nishikawa, Hitoshi Ogihara, and Ichiro Yamanaka. Liquid-Metal Indium Catalysis for Direct Dehydrogenative Conversion of Methane to Higher Hydrocarbons. *ChemistrySelect*. **2017**, 2, 4572 – 4576.

[8] Pengfei Xie, Tiancheng Pu, Anmin Nie, Sooyeon Hwang, Stephen C. Purdy, Wenjian Yu, Dong Su, Jeffrey T. Miller, and Chao Wang. Nanoceria-Supported Single-Atom Platinum Catalysts for Direct Methane Conversion. *ACS Catal*. **2018**, 8, 4044−4048.

[9] Huibo Sheng, Edward P. Schreiner, Weiqing Zheng, and Raul F. Lobo. Non-oxidative Coupling of Methane to Ethylene Using Mo2C/[B]ZSM-5. *ChemPhysChem.* **2018**, 19, 504-511.

[10] Yang Xiao and Arvind Varma. Highly Selective Nonoxidative Coupling of Methane over Pt-Bi Bimetallic Catalysts. *ACS Catal*. **2018**, 8, 2735−2740.

[11] David Bajec, Andrii Kostyniuk, Andrej Pohar, Blaž Likozar. Nonoxidative methane activation, coupling, and conversion to ethane, ethylene, and hydrogen over Fe/HZSM-5, Mo/HZSM-5, and Fe–Mo/HZSM-5 catalysts in packed bed reactor. *Int J Energy Res*. **2019**, 43, 6852–6868.

[12] Seung Ju Han, Sung Woo Lee, Hyun Woo Kim, Seok Ki Kim, and Yong Tae Kim. Nonoxidative Direct Conversion of Methane on Silica-Based Iron Catalysts: Effect of Catalytic Surface. *ACS Catal.* **2019**, 9, 7984−7997.

[13] Su Cheun Oh, Emily Schulman, Junyan Zhang, Jiufeng Fan, and Dongxia Liu. Direct Non-oxidative Methane Conversion in a Millisecond Catalytic Wall Reactor. *Angew. Chem*. **2019**, 58,7083-7086.

[14] Kanchan Dutta , Vishnu Chaudhari , Chao-Jun Li , Jan Kopyscinski. Methane conversion to ethylene over GaN catalysts. Effect of catalyst nitridation. *Applied Catalysis A, General*. **2020**, 595, 117430.

[15] Arnoldus Lambertus Dipu, Shunya Ohbuchi, Yuta Nishikawa, Shoji Iguchi, Hitoshi Ogihara, and Ichiro Yamanaka. Direct nonoxidative conversion of methane to higher hydrocarbons over silica supported nickel phosphide catalyst. *ACS Catal.* **2020**, 10, 375-379.

[16] David Bajec, Andrii Kostyniuk, Andrej Pohar, Blaž Likozar. Micro-kinetics of non-oxidative methane coupling to ethylene over Pt/CeO2 catalyst. *Chemical Engineering Journal*. **2020**, 396, 125182.

[17] Nikita Levin, Jozef Lengyel, Jan F. Eckhard, Martin Tschurl, and Ueli Heiz. Catalytic Non-Oxidative Coupling of Methane on $Ta_8O_2^+$. J. *Am. Chem. Soc*. **2020**, 142, 5862−5869.

[18] PetrŠot, Mark A. Newton, Dirk Baabe, Marc D. Walter, Alexander P. van Bavel, Andrew D. Horton, Christophe Copéret, and Jeroen A. van Bokhoven. Non-oxidative Methane Coupling over Silica versus Silica-Supported Iron(II) Single Sites. *Chem. Eur. J*. **2020**, 26, 8012 – 8016.

[19] Jianqi Haoa, Pierre Schwacha, Lulu Li, Xiaoguang Guo, Junben Weng, Hailei Zhang, Hao Shen, Guangzong Fang, Xin Huang, Xiulian Pan, Chunlei Xiao, Xueming Yang, Xinhe Bao. Direct experimental detection of hydrogen radicals in non-oxidative methane catalytic reaction. *Journal of Energy Chemistry*. **2021**, 52, 372–376.

[20] O Coufal, P Sezemsky and O Zivny, Database system of thermodynamic properties of individual substances at high temperatures. *J. Phys. D: Appl. Phys.* **2005**, *38,* 1265–1274.

[21] Baowei Wang, Wenjuan Yan, Wenjie Ge, Xiaofei Duan. Methane conversion into higher hydrocarbons with dielectric barrier discharge micro-plasma reactor. *Journal of Energy Chemistry.* **2013**, *22*, 876-882.

[22] Chao Xu, Xin Tu. Plasma-assisted methane conversion in an atmospheric pressure dielectric barrier discharge reactor. *Journal of Energy Chemistry.* **2013,** *22,* 22420–425.

[23] M. Scapinello, E. Delikonstantis, G.D. Stefanidis. Direct methane-to-ethylene conversion in a nanosecond pulsed discharge. *Fuel.* **2018**, *222*, 705–710.

[24] Faisal Saleem, Jonathan Kennedy, Usman H Dahiru, Kui Zhang, Adam Harvey. Methane conversion to H_2 and higher hydrocarbons using non-thermal plasma dielectric barrier discharge reactor. *Chemical Engineering & Processing: Process Intensification.* **2019**,*142*, 107557.

[25] E. Delikonstantis, M. Scapinello, O. Van Geenhoven, and G. D. Stefanidis, Nanosecond pulsed discharge-driven non-oxidative methane coupling in a plate-to-plate electrode configuration plasma reactor, *Chem. Eng. J*. **2020**, *380*, 122477.

[26] Galvita, V.; Siddiqi, G.; Sun, P.; Bell, A.T. Ethane dehydrogenation on Pt/Mg(Al)O and PtSn/Mg(Al)O catalysts. *J. Catal*. **2010**, 271, 209–219.

[27] Wegener, E.C.; Wu, Z.; Tseng, H.T.; Gallagher, J.R.; Ren, Y.; Diaz, R.E.; Ribeiro, F.H.; Miller, J.T. Structure and reactivity of Pt–In intermetallic alloy nanoparticles: Highly selective catalysts for ethane dehydrogenation. *Catal. Today* **2018**, 299, 146–153.

[28] Xie, Q.; Lei, T.; Miao, C.; Hua, W.; Yue, Y.; Gao, Z. Au/TiO2 for Ethane Dehydrogenation: Effect of Silica Doping. *Catal. Letters* **2020**, 150, 2013–2020.

[29] Rao, T.V.M.; Zahidi, E.M.; Sayari, A. Ethane dehydrogenation over pore-expanded mesoporous silica-supported chromium oxide: 2. Catalytic properties and nature of active sites. *J. Mol. Catal. A Chem.* **2009**, 301, 159–165.

[30] Nakagawa, K.; Kajita, C.; Ide, Y.; Okamura, M.; Kato, S.; Kasuya, H.; Ikenaga, N.O.; Kobayashiand, T.; Suzuki, T. Promoting effect of carbon dioxide on the dehydrogenation and aromatization of ethane over gallium-loaded catalysts. *Catal. Lett*. **2000**, 64, 215–221.

[31] Wang, L.C.; Zhang, Y.; Xu, J.; Diao, W.; Karakalos, S.; Liu, B.; Song, X.; Wu, W.; He, T.; Ding, D. Non-oxidative dehydrogenation of ethane to ethylene over ZSM-5 zeolite supported iron catalysts. *Appl. Catal. B Environ*. **2019**, 256, 117816.

[32] Z. Wu, B. C. Bukowski, Z. Li, C. Milligan, L. Zhou, T. Ma, Y. Wu, Y. Ren, F. H. Ribeiro, W. N. Delgass, J. Greeley, G. Zhang and J. T. Miller, Changes in Catalytic and Adsorptive Properties of 2 nm Pt3Mn Nanoparticles by Subsurface Atoms. *J. Am. Chem. Soc.*, **2018**, 140, 14870–14877.

[33] L. Wang, Y. Wang, C. W. Zhang, J. Wen, X. Weng and L. Shi, A boron nitride nanosheet-supported Pt/Cu cluster as a high-efficiency catalyst for propane dehydrogenation. *Catal. Sci. Technol.*, **2020**, 10, 1248–1255.

[34] L. L. Shen, K. Xia, W. Z. Lang, L. F. Chu, X. Yan and Y. J. Guo, The effects of calcination temperature of support on PtIn/Mg(Al)O catalysts for propane dehydrogenation reaction. *Chem. Eng. J.*, **2017**, 324, 336–346.

[35] A. WÈ©grzyniak, A. Rokicińska, E. HÈ©drzak, B. Michorczyk, K. Zeńczak-Tomera, P. Kuśtrowski and P. Michorczyk, High-performance Cr-Zr-O and Cr-K-O catalysts prepared by nanocasting for dehydrogenation of propane to propene. *Catal. Sci. Technol.*, **2017**, 7, 6059– 6068.

[36] X. Q. Gao, W. D. Lu, S. Z. Hu, W. C. Li and A. H. Lu, Rod-shaped porous alumina-supported Cr2O3 catalyst with low acidity for propane dehydrogenation. *Chin. J. Catal.*, **2019**, 40, 184–191.

[37] Y. Zhang, S. Yang, J. Lu, Y. Mei, D. He and Y. Luo, Effect of a Ce Promoter on Nonoxidative Dehydrogenation of Propane over the Commercial Cr/Al_2O_3 Catalyst. *Ind. Eng. Chem. Res.*, **2019**, 58, 19818–19824.

[38] K. M. Sundaram and G. F. Froment. Modeling of thermal cracking kinetics. 3. Radical mechanisms for the pyrolysis of simple paraffins, olefins, and their mixtures. Ind. Eng. Chem. Fundam. **1978**, 17, 174-182.